Control of the distance between porphyrin sensitizers and the TiO_2 surface in solar cells by designed anchoring groups

Carlos J. P. Monteiro [a], Patricia Jesus[a], Matthew L. Davies[b],Diana Ferreira[a], Luis G. Arnaut[a], Iluminada Gallardo[c], Mariette M. Pereira[a] and Carlos Serpa[*a]

[a]*CQC, Department of Chemistry, University of Coimbra, 3004-535 Coimbra, Portugal*

[b]*SPECIFIC, College of Engineering, Swansea University Bay Campus, Fabian Way Institution, Swansea SA1 8EN, United Kingdom*

[c]*Departament de Química, Universitat Autònoma de Barcelona, 08193-Bellaterra, Barcelona, Spain*

* Carlos Serpa: Tel: +351239852080, email: serpasoa@ci.uc.pt

Abstract: Unsymmetrical porphyrins were rationally-designed and synthesized to investigate the relation between their structure, properties and adsorption geometries, and their relative performance as dyes in dye-sensitized solar cells. Photophysics, electrochemical and TiO_2 anchoring properties of the new unsymmetrical *N*-glycolic acid amino phenyl porphyrins were evaluated. Most dyes showed good energy matching between excited state energies and the TiO_2 conduction band. Depending on the porphyrins, anchoring to TiO_2 occurred with only one carboxyl anchor group or with two N-glycolic acid amino phenyl connected to opposite and adjacent phenyl groups. It was found that cell efficiencies normalized for surface coverage are strongly affected by the adsorption geometry and spacer linker flexibility. The effective distance between the porphyrin core and the TiO_2 surface has key importance in cell efficiencies. The data is consistent with a through-space electron transfer and anchoring via N-glycolic acid substituents located in adjacent phenyl groups results in higher surface coverage normalized cell efficiencies.

Keywords: dye-sensitized solar cells; porphyrin sensitizers; anchoring mode; adjacent anchor groups; molecular efficiencies.

1. Introduction

Dye sensitized solar cells (DSSC) offer credible alternatives for the generation of electrical energy from sunlight. The first step in the modulation of a DSSC is the electronic excitation of a dye, rapidly followed by the injection of an electron into a mesoporous TiO_2 layer. Many efforts have been dedicated to the development of new sensitizers for DSSCs including organic and organometallic dye molecules. Polypyridylruthenium complexes, yielding power conversion efficiencies of ~11% with simulated sunlight, initially proved to be the most efficient sensitizers.[1-4] However, ruthenium sensitizers are expensive and have relatively low extinction coefficients in the red and near-IR regions, which limit the cost and thinness of devices. Emerging solid-state devices (ssDSSCs) require thinner photo-electrodes to allow penetration of a solid-state hole transporting material (HTM), and to benefit from lower recombination losses and higher voltages. Alternative dyes based on triarylamines,[5] indolines,[6, 7] squaraines,[5, 8] coumarins,[9] perylenes,[10, 11] phthalocyanines,[12-16] and porphyrin derivatives,[17-22] have been actively investigated.

Porphyrins are known for their role in natural photosynthetic pigments, such as chlorophylls[23, 24] and bacteriochlorophylls.[25-27] They have been quite successful in DSSC[28, 29] because of intense light absorption in the visible, relatively long singlet excited state lifetimes, appropriate redox potentials and efficient electron transfer to TiO_2. Although porphyrins tend to have relatively narrow absorption bands, their high extinction coefficients mean that a relatively low dye loading is needed to get a net positive effect when used in combination with other dyes in a co-sensitized device.[5] Another advantage of porphyrin derivatives is the plethora of possibilities for synthetic modifications. Molecular engineering of porphyrins with donor-π-acceptor configuration allowed achieving over 12% efficiencies.[30] Particularly useful is the introduction of anchoring groups and spacers on their *meso* or β-positions.[31, 32] The functionalization of porphyrins by linking an extended π-system to the *β*-position enables the extension of the β-conjugation that red shifts and broadens UV-visible bands,[33-36] and the overall efficiencies attained with such porphyrins are in the order of 7.1-7.5%.[37, 38] Impressive dyes are YD2-o-C8 and SM315, described by Grätzel and co-workers, which are based on push-pull porphyrin sensitizers with an anchoring group in the *meso* position, that reached 12.3%[29] and 13%[28] efficiencies, respectively. Although a large diversity of porphyrins have been tested in DSSCs, studies with porphyrins unsymmetrically substituted in the *meso* position remain exceptional.[31, 39-43]

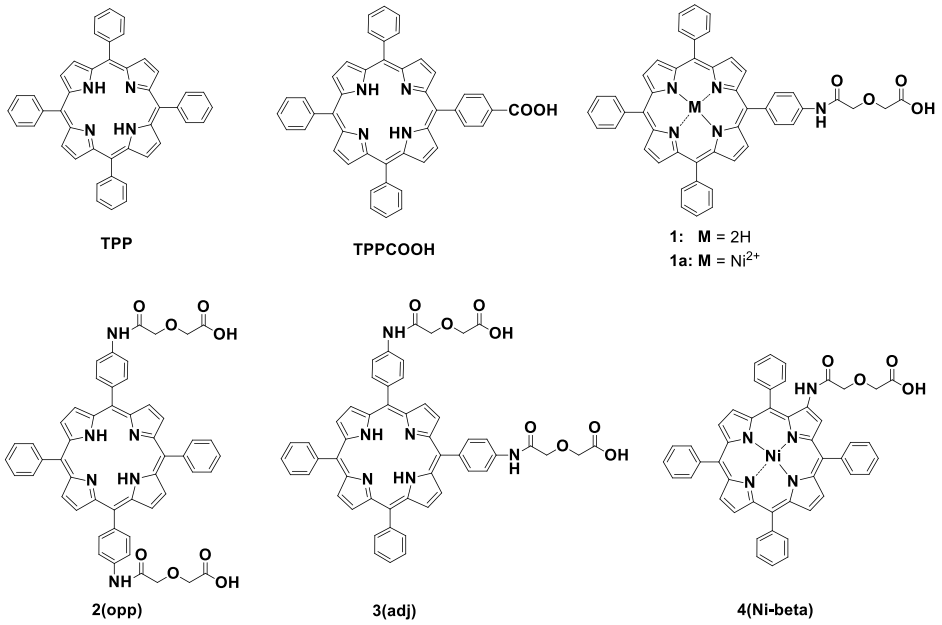

Scheme 1. Porphyrin and metalloporphyrin molecules studied on this work.

In the present study we relate the efficiencies of DSSCs with unsymmetrical *meso*-tetraphenylporphyrins with a single anchoring group, with two anchoring groups in opposite (*trans*) and adjacent (*cis*) positions, and with the same anchoring group in a *beta* position to the anchoring geometry (Scheme 1). We selected the carboxylic group to anchor the dye to TiO_2 and included a non-conjugated *N*-glycolic acid amino spacer group to increase the electron donor-acceptor separation. DSSC performance was assessed both in devices with iodide-based liquid electrolyte and with spiro-OMeTAD (2,2',7,7'-tetrakis[N,N-di(4-methoxyphenyl)amino]-9,9'-spirobifluorene) as solid-state hole conductor polymer, in view of the trend to replace liquid redox pair electrolytes by solid or *quasi*-solid hole-conduction media and avoid problems of sealing and facilitate the electron transfer at the counter electrode.[44] The device performance was assessed in terms of relative efficiencies normalized for surface coverage. The present study was performed using porphyrin dyes with good matching of the electron injection energy level with the TiO_2 conduction band, but the lessons learnt can be applied to the design of porphyrins derivatives with increased red light absorbance, such as stable chlorins and stable bacteriochlorins.[45]

2. Experimental

2.1. Porphyrin Synthesis

Commercially available chemicals were used directly without further purification. All the solvents used in the synthesis of the carboxylic acid porphyrin derivatives were purified by described methods.[46] ^{1}H-NMR spectra were recorded on a 400 MHz Bruker-Avance III. MALDI-TOF MS data were acquired using an Applied Biosystems Voyager DE-STR instrument (Framingham, MA, U.S.A.), which is equipped with a nitrogen laser and ESI-TOF MS data were obtained using a Bruker Microtof equipment. 5,10,15,20-Tetraphenylporphyrin TPP and 5-(4-carboxyphenyl)-10,15,20-triphenylporphyrin TPPCOOH were prepared by nitrobenzene method.[47, 48] The carboxylic acid derivatives 1, 2(opp), 3(adj) were prepared following the method described by Vicente and co-workers[49] and the Ni metalloporphyrin 1a(Ni), was prepared by complexation of 1 with the respective metal acetate.[50] To the best of our knowledge, compounds 1a(Ni), 2(opp) and 4(Ni-beta) were synthesized for the first time and the synthesis and full structural characterization of these compounds is described below. The synthesis of precursors nitro or amino porphyrin derivatives are described in detail in the Supporting Information section.

Preparation of 5-[4-(N-Glycolic acid-amino)phenyl]- 10,15,20-triphenylporphyrin (1).

Following the general procedure described above, 5-(4-amino)-10,15,20-triphenylporphyrin $TPPNH_2$ (100 mg; 0.159 mmol) was dissolved in dry DMF (2 mL) and diglycolic anhydride (29 mg 0.248 mmol) was added. The mixture was stirred at room temperature during 18 hours. Chloroform was added (15 mL) followed by the addition of hexane until precipitation occurs. The solid was washed with water and dried under vacuum affording 110 mg (0.147 mmol) of title compound (92% yield). The characterization obtained is in good agreement with data found in the literature.[51, 52] ^{1}H NMR (300 MHz, DMSO-d_6) δ ppm 10.50 (bs, 1H, -N*H*OCH$_2$-), 8.90 (d, 2H, *J* = 4.4 Hz, *H*-β), 8.85-8.79 (m, 6H, *H*-β) 8.26-8.12 (m, 10H, H_o-Ar+ $H_{o,m}$-Ar$_p$), 7.86-7.84 (m, 9H, $H_{m,p}$-Ar), 4.36(s, 2H, -NHOCH_2-), 4.31 (s, 2H, -CH_2COOH), -2.92 (s, 2H, N*H*). MS (MALDI-TOF), m/z: 745.23 $[M]^+$.

Preparation of 5,15- bis [4-(N-Glycolic acid-amino)phenyl]-10,20-diphenylporphyrin 2(opp).

5,15-bis(4-aminophenyl)-10,20-diphenylporphyrin (30.0 mg; 0.046 mmol) was dissolved in dry DMF (2 mL) and diglycolic anhydride (15.7 mg; 0.138 mmol) was added and stirred at room temperature for 18 hours. Chloroform was

added (15 mL), followed by the addition of hexane until precipitation occurs. The solid was washed with water and dried under vacuum affording the title compound (30.0 mg; 0.034 mmol; 76%). ^{1}H NMR (300 MHz, DMSO-d_6) δ ppm: 10.55 (bs, 2H, -N*H*OCH$_2$-), 8.90 (d, 4H, *J* = 4.6 Hz, *H*-3,7,13,17), 8.84 (d, 4H, *J* = 4.6 Hz, *H*-2,8,12,18) 8.25-8.12 (m, 12H, H_o-Ar+ $H_{o,m}$-Ar$_p$), 7.86-7.85 (m, 6H, $H_{m,p}$-Ar), 4.36 (s, 4H, -NHOCH_2-), 4.33 (s, 4H, -CH_2COOH), -2.91 (s, 2H, N*H*). HRMS (ESI-TOF) for $C_{52}H_{40}N_6O_8Na^+$: calculated m/z 899.2805, found 899.2803 [M+Na] $^+$.

Preparation of 5,10- bis [4-(N-Glycolic acid-amino)phenyl]-15,20-diphenylporphyrin (3adj).

Following the general procedure described above, 5,10-bis(4-aminophenyl)-15,20-diphenyl porphyrin TPP(NH$_2$)$_2$adj (30 mg; 0.046 mmol) was dissolved in dry DMF (2 mL) and diglycolic anhydride (15.7 mg; 0.138 mmol) was added. The mixture was stirred at room temperature during 18 hours. Chloroform was added (15 mL) followed by the addition of hexane, until precipitation occurs. The solid was washed with water and dried under vacuum affording 36.2 mg (0.041 mmol) of the title compound (90% yield). The characterization obtained is in good agreement with data found in the literature.[52] ^{1}H NMR (400 MHz, DMSO-d_6) δ ppm 10.37 (s, 2H, -N*H*OCH$_2$), 8.89 (s, 4H, *H*-3,7,8,12), 8.83 (s, 4H, *H*-2,13,17,18), 8.24-8.12 (m, 12H, H_o-Ar+ $H_{o,m}$-Ar$_p$), 7.85-7.84 (m, 6H, Ar-$H_{m,p}$), 4.37 (s, 4H, -NHOCH_2-), 4.35 (s, 4H,-CH_2COOH), -2.90 (s, 2H, N*H*).). MS (MALDI-TOF), m/z: 876.26 [M]$^+$.

Preparation of 5-[4-(N-Glycolic acid-amino)phenyl]-10,15,20-triphenylporphyrinate Ni(II) 1a(Ni).

5-[4-(N-Glycolic acid-amino)phenyl]-10,15,20-triphenylporphyrin (1 (50.0 mg; 0.067 mmol) and nickel(II) acetate tetrahydrate (167.0 mg, 0.67 mmol) were dissolved in DMF (15 mL) and stirred at 150 ℃ for 3 hours. The reaction was monitored by UV-visible spectroscopy and TLC. When completed, the reaction mixture was cooled until room temperature. Water was added slowly until precipitation. The solid was filtered under vacuum, washed with distilled water and dried, giving 48.0 mg (0.06 mmol; 89% yield) of nickel complex (II) 1a(Ni). ^{1}H NMR (300 MHz, $CDCl_3$) δ ppm: 9.28 (s, 1H, -N*H*OCH$_2$-), 8.78-8.74 (m, 8H, *H*-β), 8.01-7.95 (m, 10H, H_o-Ar+ $H_{o,m}$-Ar$_p$), 7.69-7.67 (m, 9H, Ar-$H_{m,p}$), 4.38 (s, 2H, -NHOCH_2-), 4.34 (s, 2H, -CH_2COO-), 3.88 (s, 3H, -COOCH_3). HRMS (ESI-TOF) for $C_{48}H_{33}N_5NiO_4$: calculated m/z 802.1959, found 802.1979 [M+H] $^+$. *Due to aggregation problems, the ^{1}H NMR data presented herein was obtained from the methyl ester of 1a(Ni). The methyl ester derivative of 1a(Ni) was synthesized by a method described in literature.[53]

Preparation of 2-N-Glycolic acid-amino-5,10,15,20-tetraphenylporphyrinate Ni (II) 4(Ni-beta).

To a round-bottomed flask with 2-amino-5,10,15,20-tetraphenylporphyrinate nickel (II) (50.0 mg, 0.072 mmol) in dry THF (10 mL), diglycolic anhydride (9.2 mg, 0.079 mmol) was added and the reaction was stirred at 50 ºC. The reaction was monitored by silica gel TLC and was completed in 20 hours. The solvent was removed and the residue was purified through silica gel chromatography first with acetone:methanol:triethylamine (94:5:1) as eluent, and then, with a mixture of acetone:methanol:triethylamine:acetonitrile, (50:10:10:30) to elute the compound of interest. The solid was dried, yielding the title compound (47.0 mg, 0.058 mmol, 81 % yield). ^{1}H NMR (300 MHz, $CDCl_3$) δ ppm: 9.31 (s, 1H, -N*H*OCH$_2$-), 8.99 (s, 1H, *H*-β), 8.69-8.65 (m, 4H, *H*-8,12,13,17), 8.62 (d, *J* = 4.9 Hz, 1H, *H*-β), 8.42 (d, *J* = 4.9 Hz, 1H, *H*-β), 7.97-7.89 (m, 8H, H_o-Ar), 7.68-7.61 (m, 12H, $H_{m,p}$-Ar), 4.04 (s, 2H, -NHOCH_2-), 3.85 (s, 2H, -CH_2COOH). HRMS (ESI-TOF) for $C_{48}H_{34}N_5NiO_4$: calculated m/z 802.1959, found 802.1958 [M+H]$^+$.

2.2. Absorption and fluorescence

Steady-state absorption and fluorescence were recorded with Shimadzu UV-2100 and Horiba-Jobin-Yvon-SPEX Fluorolog 3-22 spectrometers, respectively. Fluorescence quantum yields (Φ_F) were determined using deaerated ethanol porphyrin solutions and TPP in toluene as fluorescence standard (Φ_F = 0.11).[54] Φ_F was calculated by comparison of the sample and reference integrated fluorescence spectra after correction for the difference in refractive index of toluene and ethanol ($\eta_{toluene}$ = 1.49693 and $\eta_{ethanol}$ =1.36168),[54] using solutions with 0.02 absorbance at 418 nm.

2.3. Excited state lifetimes

Fluorescence lifetimes were measured with a previously described homebuilt apparatus by using an IBH5000 coaxial flashlamp, filled with N_2, D_2, or H_2 gases (or mixtures of them), or an IBH nanoLED (281, 339, 373 nm), as excitation source, Philips XP2020Q photomultiplier, with excitation and emission wavelengths selected with Jobin–Yvon H20 monochromators, and a Canberra Instruments time-to-amplitude converter and multichannel analyser.[55] Alternate measurements (1000 counts per cycle at the maximum) of the pulse profile and the sample emission were performed until 5R103 counts at the maximum were reached. The fluorescence decays were analyzed by using Striker's method of modulating functions, with automatic correction for the photomultiplier "wavelength shift".

2.4. Electrochemistry

Cyclic voltammetric measurements were carried out in a VSP electrochemical potentiostat at 0.05 and 0.5 V s^{-1} scan rates, using a conical cell to set-up the three electrodes system. A glassy carbon working electrode, with a diameter of 0.5 mm, was employed. It was polished using 1 μm diamond paste after each experiment. The counter electrode was a 1 mm diameter Pt disk. Standard potentials were determined at room temperature with 0.5 mM porphyrin solutions prepared in 1,2-dichloroethane (DCE) containing 0.10 M tetrabutylammonium hexafluorophosphate ($TBAPF_6$). DCE was neutralized with neutral activated alumina just before use. The solutions were purged with argon before the measurements were made, and the gas was allowed to flow above the solution during the measurements. All the potentials are reported *vs* an aqueous saturated calomel electrode (SCE) isolated from the working electrode compartment by a salt bridge. The salt solution of reference calomel electrode was separated from the electrochemical solution by a salt-bridge ended with a frit, which was made of a ceramic material, allowing ionic conduction between the two solutions but avoiding contamination. The solvent/supporting electrolyte present in the salt bridge was the same used for the electrochemical solution, minimizing junction potentials (DCE + 0.10 M $TBAPF_6$). Fluorenone (E^0= -1.26V vs SCE; $1e^-$) and tris-4-bromophenylamine (E^0= +1.38 V vs SCE; $1e^-$) were used as external standards for reduction and oxidation, respectively.

2.5. Adsorption

TiO_2 films for adsorption studies were prepared by screen printing. Titanium dioxide paste from Solaronix (Ti-Nanoxide HT/SP, 8-10 nm particles) was deposited on a glass slide by screen printing an area of 1 cm^2. The resulting films were gradually heated with the following heating profile: 125 ºC for 10 min, 325 ºC for 5 min, 375 ºC for 10 min, 450 ºC for 10 min and 500 ºC for 15 min. Morphology and thickness of the TiO_2 films (1.2 μm) was measured by SEM.

Porphyrin solutions ($5x10^{-5}$ M) were prepared in THF, TiO_2 films were immersed in the solutions, and absorption spectra were taken at selected time intervals from 20 sec to 180 min. The excess of dye was removed by rinsing with solvent prior to measurement. Experiments were performed at 20 ºC. The amount of adsorbed dye was monitored as a

function of time by measuring the absorbance of the dye-modified TiO_2 films at the porphyrins Q bands using a Shimadzu UV-2450 spectrophotometer. For the desorption studies, a few drops of NaOH (0.1 M) were deposited on the films and then these were immersed in THF (3 mL). The total amount of dye adsorbed on the TiO_2 films was determined by measuring the absorbance of the THF solution.

2.6. Device manufacture and characterization

The working photoelectrode was prepared by doctor blading a thin film of commercial titania colloid (18NR-AO Active Opaque Titania Paste, Dyesol) onto TEC 15 glass using a single layer of Scotch tape (3M) as spacer. Films were sintered at 450 °C for 30 minutes. Electrodes were immersed in $TiCl_4$:THF in deionised water (40 mM) at 70 °C for 30 min, rinsed with deionised water, air-dried for 10 min and re-sintered at 450 °C for 30 min, yielding TiO_2 films with estimated thickness of ca. 7 μm. Solutions containing dye (5 mM) and chenodeoxyxcholic acid (10 mM, Aldrich)[16] were prepared in THF. After dyeing, a Surlyn® (Du Pont) gasket was placed around the photo-electrode and a Pt-coated TEC 8 counter electrode which had been treated with Pt paste (PT1, Dyesol) and heated to 400 ºC was placed on top and the two electrodes sealed together at 120 °C. Electrolyte containing iodine/tri-iodide (I_2 100 mM in acetonitrile) was added through a hole in the counter electrode which was then sealed using Surlyn®. For the ssDSSC the working photoelectrode was prepared by spin coating a thin film of commercial titania colloid (18NR-AO Active Opaque Titania Paste, Dyesol) diluted 1:2 with EtOH onto TEC 15 glass. Films were sintered at 450 °C for 30 minutes and placed into the dye solution overnight. After dyeing and drying, a spiro-OMeTAD HTM was spin coated onto the photoelectrode. Finally a ca. 60 nm Au metal contact was thermally evaporated onto the HTM layer to complete the device. Current–voltage characteristics were measured with an ABET Solar Simulator with a Xe arc lamp and a Keithley 2400 at 100 mW cm^{-2} between 0 and 1 V. Spectral response measurements were made from 300–800 nm either on a QEX10 Quantum Efficiency Measurement System or on a QE/IPCE system from Newport in DC mode at a resolution of 2 nm.

3. Results and discussion

3.1. Synthesis

Although alternative groups, e.g. alcohols,[56] have been proposed for dye-TiO_2 linkage, it is established that the best anchoring groups to adsorb onto the TiO_2 surface of a DSSC, are carboxylic acid groups.[57-59] It is also know that a spacer between the dye and the semiconductor surface is necessary to control and ultimately avoid losses related with back electron transfer.[58, 60] Our strategy to obtain the *meso*-aryl porphyrins dyes 1, 2(opp), 3(adj) with appropriate *meso*-phenyl spacer and carboxylic acid anchoring groups, was based on a method described by Vicente and co-workers[49] and is represented in Scheme 2.

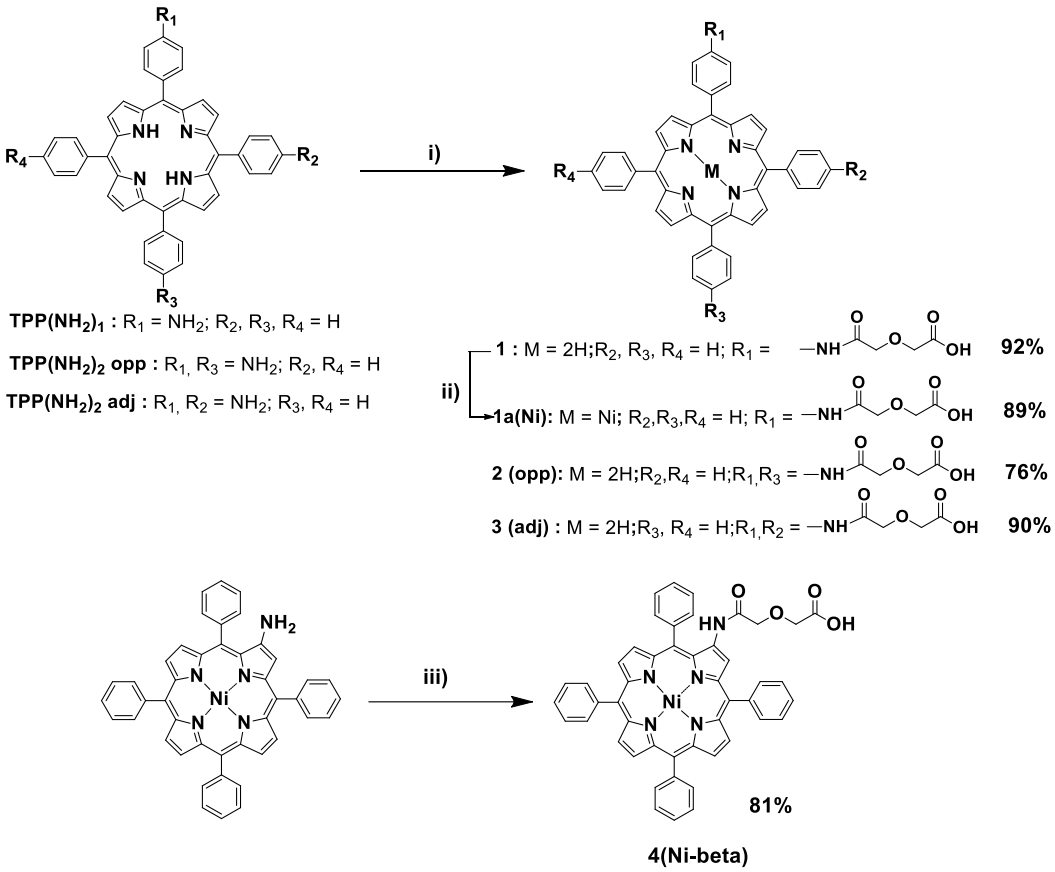

Scheme 2. Synthesis strategy with the following reaction conditions: i) diglycolic anhydride, DMF, room temperature, 18 hours; ii) $Ni(CH_3COO)_2$, DMF, 3 hours; iii) diglycolic anhydride, THF, 50ºC, 20 hours.

The reaction of mono and di-substituted amine-porphyrins with diglycolic anhydride gave the corresponding mono and di-carboxylic porphyrins 1, 2(opp) and 3(adj) with 92%, 76% and 84% yields, respectively. The porphyrin regioisomers 2(opp) and 3(adj)) show the characteristic splitting pattern for the resonance of β-pyrrolic protons in ^{1}H NMR spectra, which allowed us to distinguish the two compounds. The eight β-protons for *cis* regioisomer, 3(adj) appear as two singlets at 8.89 (4H) and 8.83 (4H) ppm, whereas for *trans* regioisomer, 2(opp), the eight β-protons appears as two doublets at 8.90 and 8.84 with a coupling of *J*=4.6 Hz, distinctive of β-H/β-H coupling constant of highly symmetrical di-substituted porphyrins The modulation of porphyrin dye redox properties was made by the introduction of a nickel metal on the porphyrin core. The nickel 1a(Ni) metal complex was prepared by refluxing the monocarboxylated porphyrin 1 in DMF with an excess of metal acetate[50] $Ni(CH_3COO)_2$ with 89% yield, Scheme 2. The introduction of *N*-glycolic acid amino group on the β-position of TPP was carried out by mono nitration of the β–pyrrolic position using copper nitrate/acetic anhydride as nitrating agent. When TPP reacts with copper nitrate trihydrate/acetic anhydride/acetic acid in $CHCl_3$ at 40 ºC,[61, 62] the simultaneous preparation of the CuTPP complex and the β–nitration occurs yielding 2-nitro-5,10,15,20-tetraphenylporphyrinato copper (II) (79% yield). Demetalation with sulfuric acid/chloroform affords the free base 2-nitro-5,10,15,20-tetraphenylporphyrin with 76 % yield. Since our intent was the reduction of the β-nitro group, 2-nitro-5,10,15,20-tetraphenylporphyrin was complexed with nickel, and the previously prepared β-nitrated nickel complex was reduced with tin powder/HCl,[63] and then the β-aminated porphyrin derivative was dissolved in THF and reacted with diglycolic anhydride yielding 2-*N*-glycolic acid-amino-5,10,15,20-tetraphenylporphyrin 4(Ni-beta) (81% yield), Scheme 2. The ^{1}H NMR spectrum of 4(Ni-beta) shows the typical singlet

resonance at 8.99 ppm assigned to the β-pyrrolic proton (H-3) next to the amide group, whose NH proton appears at 9.31 ppm.

3.2. Optical properties

Table 1. Electronic absorption and emission parameters in solution.

Sensitizer	Absorption[a] λ_{max} / nm (ε / $M^{-1}cm^{-1}$)					Fluorescence[b] λ_{max} / nm		E_S[c] / eV	Φ_F[b]	τ_S / ns
	B(0-0)	Q_x(1-0)	Q_x(0-0)	Q_y(1-0)	Q_y(0-0)	Q(0-0)	Q(0-1)			
TPP	418 ($2.7x10^5$)	514 ($1.8x10^4$)	548 ($1.2x10^4$)	592 ($1.0x10^4$)	650 ($9.6x10^3$)	653	718	1.91	0.11	12.6
TPPCOOH	418 ($2.8x10^5$)	514 ($1.3x10^4$)	556 ($7.5x10^3$)	591 ($4.0x10^3$)	648 ($3.4x10^3$)	650	716	1.92	0.088	10.0
1	418 ($3.6x10^5$)	515 ($1.3x10^4$)	550 ($6.4x10^3$)	589 ($4.0x10^3$)	646 ($3.1x10^3$)	650	715	1.92	0.085	10.0
1a(Ni)	413 ($1.7x10^5$)	528 ($1.5x10^4$)	---	---	---	---	---	2.19	---	---
2(opp)	418 ($2.8x10^5$)	514 ($1.3x10^4$)	556 ($7.5x10^3$)	591 ($4.0x10^3$)	648 ($3.8x10^3$)	652	716	1.91	0.063	9.3
3(adj)	418 ($1.5x10^5$)	515 ($6.5x10^3$)	550 ($3.8x10^3$)	591 ($2.0x10^3$)	648 ($1.8x10^3$)	652	715	1.91	0.079	10.0
4(Ni-beta)	413 ($3.3x10^5$)	529 ($1.9x10^4$)	565 (shoulder)	609 ($1.8x10^3$)	---	---	----	1.86	---	---

[a]Absorption data (ε) for TPPCOOH, 1, 1a(Ni) and 4(Ni-beta) were obtained in DCM, 2(opp) and 3(adj) in THF and TPP in toluene. [b]Steady state fluorescence and singlet lifetimes (τ_s) were measured in ethanol for all the compounds, except for 1a(Ni) that was measured in THF. [c]The singlet state energies (E_S) were obtained from the crossing of the absorption spectra lowest energy Q band **(in solvent)**, with the highest energy Q band, **from** the emission spectra **(in solvent)**, except for compounds 1a(Ni) and 4(Ni-beta) where E_S were predicted from the maximum of the estimated vibrational progression of the longest wavelength band.

The UV-Vis absorption, fluorescence and singlet lifetime data of the studied carboxylic porphyrin and metalloporphyrins dyes are presented in Table 1. Molar absorption coefficients were calculated from the UV-Vis spectra measured in DCM or THF. The UV-Vis spectra obtained for these compounds in solution, exhibit typical behavior found for tetrapyrrolic macrocycles comprising an intense Soret band in the 400-450 nm range and Q bands from 500-650 nm with lower intensities. Table 1 show that the carboxylic group in the periphery of TPPCOOH does not cause a significant perturbation on the UV-Vis spectra when compared with TPP. The introduction of a spacer between the phenyl group and the carboxylic group, i.e., porphyrin 1, does not affect the electronic properties of porphyrin 1 when compared with TPPCOOH. The complexation of 1 with Ni (1a(Ni)) changes the four Q bands of the free base 1 into one single observable band in the Ni complex,[64] due to the higher symmetry of the metalloporphyrin.[65, 66] Additionally, complexation with nickel leads to a blue shift (5 nm) of the Soret band. This shift is typical for metals with partially filled *d* orbitals (d^8) due to an interaction of the metal ion *d* orbital with the porphyrin aromatic π system. The 4(Ni-beta)) shows three absorption bands, extended to 650 nm, indicating that the β-functionalization interferes with the central metal symmetry enhancement.[67] The UV-Vis spectra of porphyrin 1, the nickel metal complexes (1a(Ni) and 4(Ni-beta)) and the disubstituted porphyrins 2(opp) and 3(adj), are shown in Figure 1.

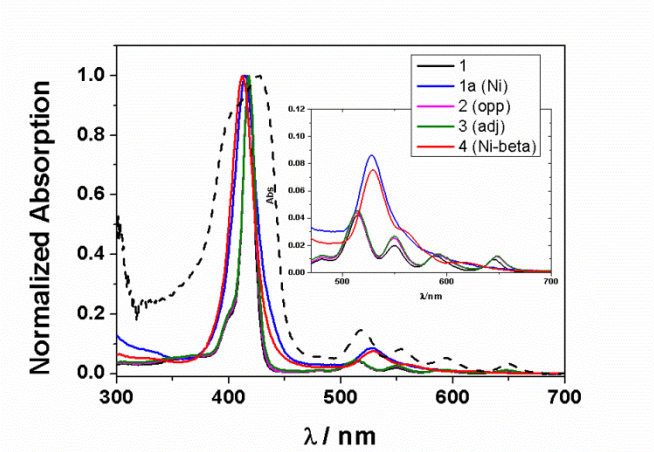

Fig. 1. Normalized UV-VIS absorption spectra of the carboxylated meso-phenyl substituted porphyrin 1, nickel complex (1a(Ni)), β–substituted Ni complex (4(Ni-beta)), disubstituted porphyrins 2(opp) and 3(adj), measured in dichloromethane; porphyrin 1 adsorbed in TiO_2 film in dashed line.

The absorption maxima obtained for disubstituted carboxylic porphyrins 2(opp) and 3(adj) are very similar between them and almost coincident with the UV-Vis spectra for the mono-substituted porphyrin 1. However, the molar absorption coefficients of the adjacent isomer 3(adj) are about half of the value obtained for the opposite isomer 2(opp), being the later values very close to the porphyrin 1. This fact could be explained by aggregation, as porphyrin 3(adj) is more polar than porphyrin 2(opp), but the molar absorption coefficients were determined at low dye concentrations. A more plausible explanation may be related with dipole transition moment. The porphyrin 2(opp) has a higher symmetry than porphyrin 3(adj) and may have a lower dipole transition moment, influencing the molar absorption coefficients. The UV-Vis spectra of the β-substituted nickel metalloporphyrin 4(Ni-beta) (Figure 1) does not show either a significant shift to the red nor a broadening when compared to 1a(Ni), since the spacer introduced is not conjugated with the porphyrin ring. The emission data are present in Table 1 and the fluorescence spectra are shown in the Supplementary Material.

The fluorescence quantum yields and the singlet state lifetimes measured for the free base porphyrins 1, 2(opp) and 3(adj) are very similar to the values measured for TPPCOOH, which indicates that the introduction of spacers onto the peripheral phenyl rings does not affect significantly the singlet state properties. In our experimental conditions, no fluorescence emission was detected for nickel complexes, 1a(Ni) and 4(Ni-beta). This is assigned to the fast thermal deactivation to the ground state, as described in literature for nickel complexes.[65, 68]

The free base porphyrins singlet state energies (E_S) in Table 1, were calculated from the intersection of normalized fluorescence and emission spectra. The E_S values of all the free-base porphyrins were very similar (between 1.91 and 1.92 eV). The values for nickel complexes 1a(Ni) and 4(Ni-beta) could not be obtained directly from experimental data, since not only no emission was detected for these compounds irrespective of the excitation wavelength used, but also the observed absorption Q band corresponds to a transition to a vibrational excited state, Q (1,0). The values for nickel complexes 1a(Ni) and 4(Ni-beta) were obtained using the maximum of the estimated vibrational progression of the respective lowest energy Q band observed. Compared with the corresponding free bases, the Ni complexes 1a(Ni), 4(Ni-beta) E_S (2.19 eV and 1.86 eV) correspond to a balance between the symmetry enhancement due to the presence of the central metal and the symmetry decrease due to single β-functionalization. Luminescence quenching is an indication photoinduced charge transfer occurs between the dye and TiO_2 nanoparticles.[15, 69] We do not find evidence extensive dye aggregation upon adsorption. Although quenched, we still observed residual steady state emission from dye 1 and 3(adj) when adsorbed on highly transparent TiO_2 films. The singlet state of these porphyrins is not totally quenched by

nanoparticulate TiO_2. With reduced intensity[20] or fluorescence lifetime[70] other reports have also showed persistent emission of free base porphyrins adsorbed in TiO_2.

3.3. Electrochemical studies

The electrochemical properties of these porphyrins were investigated using cyclic voltammetry (CV). The studies were carried out in 1,2-dichloroethane (DCE) for all the porphyrins except for 2(opp) and 3(adj) due to their low solubility in DCE. The first oxidation (E^0_{ox}) and the first reduction (E^0_{red}) standard potentials are collected in Table 2 and their cyclic voltammograms are available in Supplementary Material. E^0_{ox} and E^0_{red} are representative of the energy of molecular orbitals HOMO and LUMO involved in the electron transfer process in DSSCs. Only TPP presents two well-defined cathodic and two well-defined anodic waves. However, it is possible to measure the values of the first oxidation (E^0_{ox}) and the first reduction (E^0_{red}) standard potentials for all the porphyrins investigated.

Table 2. Electrochemical data and electron transfer processes driving forces for the studied porphyrin dyes.

Sensitizer	E^0_{red}[a]/V	E^0_{ox}[a]/V	$\Delta E_{HOMO-LUMO}$[b]/V	E^0_{ox}*[c]/V	ΔG_{CS}[d]/eV	ΔG_{reg}[e]/eV	ΔG_{reg}[f]/eV
TPP	-1.23	0.98	2.21	-0.93	-0.19	-0.72	-0.49
TPPCOOH	-1.21	1.10	2.31	-0.82	-0.08	-0.84	-0.61
1	-1.22	0.98	2.20	-0.94	-0.20	-0.72	-0.49
1a(Ni)	-1.33	1.02	2.35	-1.17	-0.43	-0.76	-0.53
2(opp)[h]	**<-0.97**[g]	**0.92**	**>1.89**	**-0.99**	**-0.25**	**-0.66**	**-0.43**
3(adj)[h]	**<-1.98**[g]	**0.99**	**>1.97**	**-0.92**	**-0.18**	**-0.73**	**-0.49**
4(Ni-beta)	-1.27	1.00	2.34	-0.86	-0.12	-0.74	-0.51
TPP	-1.23	0.98	2.21	-0.93	-0.19	-0.72	-0.49

[a]Standard Potentials vs SCE. [b]$\Delta E_{HOMO-LUMO}=E_0^{ox}-E_0^{red}$. [c]$E_0^{ox*}=E_0^{ox}-E_S$. [d]Driving force for electron injection from the first singlet excited state (E_0^{ox*}) to the conduction band of TiO_2 (-0.74 V vs SCE). [e]Driving force for radical cation porphyrin regeneration (E_0^{ox}) by redox couple I^-/I_3^- (+0.26 V vs SCE) or [f]by hole transporter spiro-OMETAD (+0.49 vs SCE). [g]For irreversible processes, the potentials were estimated by the cathodic peak potential, E_{PC}. [h]Solvent: THF. The data for TPP, TPPCOOH, 1, 1a(Ni), and 4(Ni-beta) were obtained in DCE.

Table 2. Electrochemical data and electron transfer processes driving forces for the studied porphyrin dyes.

Sensitizer	E^0_{red}/V [a]	E^0_{ox}/V [a]	ΔEHOMO-LUMO [b] /V	E^0_{ox}*[c]/V	ΔG_{CS}[d]/ eV	ΔGreg [e] /eV	ΔG_{reg}[f]/eV
TPP	-1.23	0.98	2.21	-0.93	-0.19	-0.72	-0.49
TPPCOOH	-1.21	1.10	2.31	-0.82	-0.08	-0.84	-0.61
1	-1.22	0.98	2.20	-0.94	-0.20	-0.72	-0.49
1a(Ni)	-1.33	1.02	2.35	-1.17	-0.43	-0.76	-0.53
4(Ni-beta)	-1.27	1.00	2.34	-0.86	-0.12	-0.74	-0.51

[a] Standard Potentials *vs* SCE. [b]$\Delta E_{HOMO-LUMO} = E^0_{ox}-E^0_{red}$. [c] $E^0_{ox}*=E^0_{ox}-E_S$. [d] Driving force for electron injection from the first singlet excited state (E^0_{ox}*) to the conduction band of TiO_2 (-0.74 V *vs* SCE). [e] Driving force for radical cation porphyrin regeneration (E^0_{ox}) by redox couple I^-/I^{3-} (+0.26 V *vs* SCE) or [f] by hole transporter spiro-OMETAD (+0.49 vs SCE).

Results in Table 2 show in some cases that the first oxidation (E^0_{ox}) and the first reduction (E^0_{red}) standard potentials of porphyrins are shifted with respect to that of TPP. Thus, TPPCOOH shows an anodic shift of +0.12 V for the first

oxidation, E^0_{ox}, when compared to TPP, while the cathodic shift for the first reduction E^0_{redn} is almost negligible. The introduction of spacer between the phenyl ring and the carboxylic group in porphyrin 1, brings E^0_{ox} and E^0_{ox} nearly identical to that of TPP. The introduction of nickel in the porphyrin 1, giving 1a(Ni), did not significantly affect the E^0_{ox} (+0.04 V anodic shift), but a cathodic shift of -0.11 V was observed with respect to the free porphyrin 1. Very small shifts in the redox potentials were found in nickel β-substituted porphyrin 4(Ni-beta) compared with the 1a(Ni) substituted at the meso position of the phenyl ring. This fact means that the presence of a spacer between a functional group and the porphyrin ring, either at β- or at the meso phenyl positions, does not produce a significant perturbation of the electronic π system of the macrocycle and, consequently, the ΔE between HOMO and LUMO orbitals is preserved. This observation is in good agreement with the UV-Vis spectra of 4(Ni-beta) and 1a(Ni) porphyrins.

The electron injection from the adsorbed porphyrins to the TiO_2 semiconductor, as well as the porphyrin radical cation regeneration by the redox shuttle I^-/I_3^- or hole transporter spiro-OMeTAD, takes place efficiently when the driving force is appropriate for those processes. In order to assess the driving forces for both processes, we calculate the excited state oxidation potentials (E^0_{ox}*) from the first oxidation potential (E^0_{ox}) and from the singlet excited state energy (*ES*), Table 1. These values and the potential for the conduction band of TiO_2 (-0.74 V vs SCE), [71, 72] allowed us to calculate the electron injection driving forces, ΔG_{CS}. The dye regeneration driving forces (ΔG_{reg}) were also estimated with the first oxidation potential (E^0_{ox}) of the dye and the redox couple $I^-/_{I3}^-$ or the hole transporter spiro-OMeTAD potentials (0.26 V and 0.49 vs SCE), [71, 72] Table 2 and Figure 2. The driving force values calculated for the dye cation regeneration (ΔG_{reg}) were thermodynamically favourable for all the porphyrins studied. For the electron injection process, the metal complex 1a(Ni), showed the highest driving force (-0.43 V) whereas driving force values are consistently lower for the remaining dyes (ΔG_{CS} < -0.2 V), which is desirable for harvesting solar energy.[73] In this regard, it is worth noting that TPPCOOH leads to the lowest electron injection driving force. We notice that those LUMO levels were not measured on a TiO_2 surface, which is known to shift the energy level positions. Additionally, the use of chenodeoxycholic acid, co-adsorbent in cells to reduce aggregation effects, is known to shift TiO_2 potentials.[69] Thus, those dyes LUMO energy levels are mostly an indication of the relative energies between the sensitizers. Moreover, electron transfer from adsorbed dyes to TiO_2 can be very fast and at least partly occur from upper vibrational states of the singlet state.[74] Matching the energy level of the dye with the TiO_2 conduction band is a crucial aspect for the solar cell application; if the LUMO level is too low in energy, and it lies below the conduction band edge, then electron transfer will be retarded; too high energy level in the dye will require high energy light to be excited thus reducing the light harvesting efficiency across the visible region.

Analyzing Table 2, we can see that TPPCOOH shows an anodic shift of +0.12 V for the first oxidation peak, when compared to TPP, while the cathodic shift for the first reduction potential peak for TPPCOOH is almost negligible. The introduction of a spacer between the phenyl ring and the carboxylic group in porphyrin 1 brings the oxidation potential to a value very similar to that of TPP. Conversely, the introduction of a second spacer, bearing a carboxylic group, in an opposite phenyl ring (porphyrin 2(opp)) or in an adjacent phenyl ring (porphyrin 3(adj)) results in a remarkable shift for oxidation and reduction potentials comparatively to compound 1. For porphyrin 3 an anodic shift of 0.24 V was found for the first oxidation potential when compared with porphyrin 1. In reduction, a cathodic shift 0.15 V was observed for the first reduction peak comparing with porphyrin 1. A similar behavior was found for compound 2, but in that case the anodic shift for E^0_{ox} was 0.17 V and the cathodic shift for E^0_{red} was 0.16 V. The introduction of nickel on the porphyrin 1, giving 1a(Ni), did not significantly affect the oxidation potential (0.04 V anodic shift). In the reduction a cathodic shift of 0.11 V was found for 1a(Ni). Significant shifts in redox potentials were not found when the nickel β-substituted porphyrin 4(Ni-beta) was compared with the 1a(Ni) substituted on the meso position of the phenyl ring. This fact means that the spacer directly linked to the porphyrin ring is not perturbing significantly the macrocycle electronic π system and consequently, the HOMO and LUMO orbitals. This observation is in good agreement with the UV-Vis spectra of compounds (4(Ni-beta)) and (1a(Ni)).

The electron injection from the adsorbed porphyrins to the TiO_2 semiconductor, as well as the porphyrin radical cation regeneration by the redox shuttle I^-/I_3^- or hole transporter spiro-OMeTAD takes place efficiently when the

driving force is appropriate for those processes. In order to assess the driving forces for both processes, we calculate the excited state oxidation potentials (E^0_{ox}*) from the first oxidation potential (E^0_{ox}) and from the singlet exited state energy (E_S), Table 2. These values and the potential for the conduction band of TiO_2 (-0.74 V vs SCE),[71, 72] allowed us to calculate the electron injection driving forces, ΔG_{CS}. The dye regeneration driving forces (ΔG_{reg}) were also estimated with the first oxidation potential (E^0_{ox}) of the dye and the redox couple I^-/I_3^- or the hole transporter spiro-OMeTAD potentials (0.26 V and 0.49 vs SCE),[71, 72] Table 2 and Figure 2. The driving force values calculated for the dye cation regeneration (ΔG_{reg}), were thermodynamically favourable for all the porphyrins studied. For the electron injection process, the metal complex 4(Ni-beta), showed the higher driving force (-0.43 V) whereas driving force values are consistently lower for the remaining dyes (ΔG_{CS}<-0.25 V), **a consequence of the reduced band gap of the dyes and desirable for harvesting solar energy over a broader wavelength range.**[73] In this regard it is worth noting that apparently the extra linker on dyes 2(opp) and 3(adj) leads to electron injection driving forces **near zero**. We notice that those LUMO levels were not measured on a TiO_2 surface, which is known to shift the energy level positions. Additionally the use of chenodeoxyxcholic acid co-adsorbent in cells, in order to reduce aggregation effects, is known to shift TiO_2 potentials.[69] Thus, those dyes LUMO energy levels are mostly an indication of the relative energies between the sensitizers. Moreover, electron transfer from adsorbed dyes to TiO_2 can be very fast and at least partly occur from upper vibrational states of the singlet state.[74] Matching the energy level of the dye with the TiO_2 conduction band is vital; if the LUMO level is too low, in energy terms, and below the conduction band edge then electron transfer will be retarded; too high and it will require higher energy light to be excited thus reducing the light harvesting efficiency across the visible region.

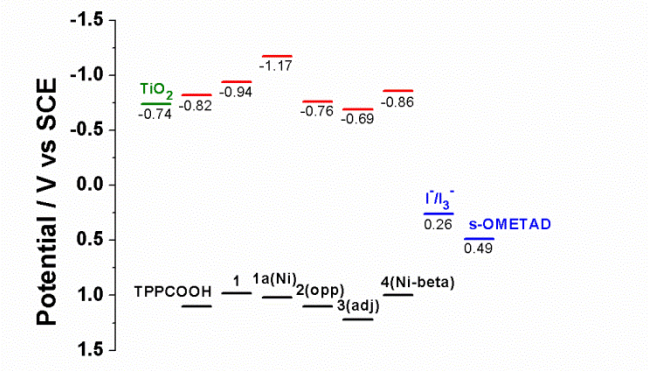

Fig. 2. Energy level diagrams of the porphyrins studied.**CHANGE**

3.4. Porphyrin Adsorption on TiO_2

The UV-vis absorption spectra of Ni porphyrins did not change upon adsorption, while the Soret and Q bands of some free-bases did change, as exemplified in Figure 1. The Q bands of TPPCOOH, 1, 2(opp), 3(adj) exhibited small red shift together with a split and broadened Soret band. This was more notorious in TPPCOOH and can be attributed to excitonic interaction in densely packed monolayers adsorbed on the TiO_2 surface.[75] The geometry of the porphyrin macrocycle with respect to the TiO_2 nanoparticulate surface, here denominated as the anchoring mode, is known to influence cell efficiency.[31] The efficient performance of Ru DSSC may partly originate from the robust adsorption of ruthenium dyes on the TiO_2 through more than two anchoring groups.[75] The flexible geometry of porphyrins adsorbed on the TiO_2 surface through only one anchoring group may render the cell performance more susceptible to substituents

and adsorption conditions. The nature of the solvent used for adsorption might also influence the adsorption kinetics and thermodynamics, and influence the sensitizers geometry on the TiO_2 surface.[76] Indeed, cell performances of porphyrin sensitized solar cells show a strong dependency on both the immersing solvents and immersing times.[75] Protic and non protic solvents have been used and in some cases ethanol or methanol resulted in superior performance DSSC.[75] Some of the porphyrin dyes used here do not properly dissolve in ethanol and thus THF was used as the immersing solvent for all porphyrins.

We employed low porphyrin concentrations ($5x10^{-5}$ M) and 1.2 μm thick TiO_2 films with 1 cm^2. The available TiO_2 surface area was calculated using the specific surface area for the TiO_2 nanoparticles (160 m^2 g^{-1} obtained considering BET theory) and the measured mass of the films. The adsorbed porphyrin density (Γ) was then calculated from the quantity of porphyrin adsorbed after reaching adsorption saturation and is presented in Table 3. All porphyrins reach TiO_2 surface coverage saturation within 1.5 h of immersion (Figure 3). Experimental adsorption times (τ) and adsorption rates in Table 3 were obtained by the adjustment of a pseudo-first order Lagergren's equation.[60] Initial adsorption rate is notable faster for 4(Ni-beta), which is linked to a position of the ring, and 3(adj), which as two anchoring groups linked to adjacent positions of a phenyl ring. The porphyrin with anchoring groups at opposite *meso* positions, 2(opp), shows a relatively slow adsorption, and the lower adsorption rate was observed for 1a(Ni), that has only one anchoring group.

Table 3. Adsorption kinetics (τ, k_{ads}), experimental saturated dye density on TiO_2 (Γ) and area occupied by one dye molecule at TiO_2 surface (A_{dye}).

Sensitizer	τ / min	k_{ads} / min^{-1}	Γ / 10^{-11} mol cm^{-2}	A_{dye}[a] / $Å^2$
TPPCOOH	18.7	0.056	7.2	230
1	25.7	0.042	10.4	160
1a(Ni)	33.9	0.032	6.2	268
2(opp)	27.4	0.037	10.3	161
3(adj)	10.5	0.095	4.9	339
4(Ni-beta)	10.8	0.095	6.0	277

[a]Assuming homogenously packed porphyrin coverage on the TiO_2 surface.

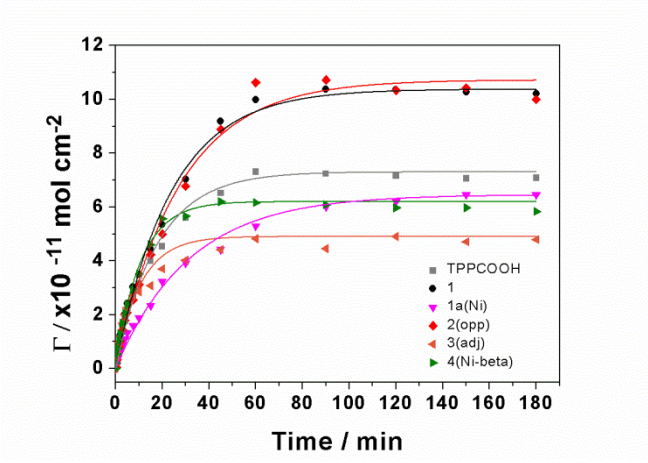

Fig. 3. Porphyrin surface coverage density on TiO_2 particles (Γ) as a function of immersion time at room temperature.

The adsorption rate differences observed here cannot be assigned to distinct electron densities on anchor or spacer groups,[77] as all porphyrins (with exception of TPPCOOH) have the same non-conjugated *n*-glycolic acid amino spacer group. They more likely arise from distinct adsorption geometries. The presence of an anchoring group in one phenyl ring or two opposite phenyl rings, in porphyrins TPPCOOH, 1, 1a, and 2(opp), does not change the initial adsorption rates appreciably, but the presence of anchoring groups in adjacent phenyl rings in 3(adj) approximately doubles the initial adsorption rate. On the other hand, similar maximum adsorption densities were obtained for porphyrins 1 and 2(opp), and they are twice as large as that of 3(adj). The similarity in adsorption rates and surface coverage of 1 and 2(opp) suggests that these porphyrins adsorb to the surface with a vertical geometry, perpendicular to the TiO_2 surface, maximizing surface coverage. The faster initial adsorption rate and lower surface density coverage of 3(adj) probably reflects the use of two anchoring groups to adsorb to TiO_2 and flatter adsorption geometry. A lower adsorption density was also reported for a porphyrin with anchor groups connected by two adjacent carboxyphenyl linkers compared with a porphyrin with only one of such linkers.[78] The comparison between 1 and 1a(Ni) shows that the presence of the metal tends to lower both the initial adsorption rate and the surface density coverage. This is unlikely to be related to the size of the Ni atoms but may be related to the ability of this metal to take the carboxylic acid anchor group as an axial ligand and hinder adsorption. Interestingly, this does not seem to occur with 4(Ni-beta) presumably because of the shorter distance between the metal and the carboxylic group. The Ni complexes have lower maximum adsorption densities than what could be expected from the presence of only one anchoring group. This lower surface coverage of the Ni complexes can also be tentatively assigned to possible interactions between the metal atom and the Si=O groups at the surface of the nanoparticles, leading to a more tilted geometry. Finally, TPPCOOH has a relatively small adsorption compared with 1, which can be related with the higher steric hindrance associated with the loss of flexibility of the linker. The relative values of k_{ads} and Γ support the adsorption geometries proposed in schematic form at Figure 4.

The effective area occupied by one dye molecule at TiO_2 surface, A_{dye}, was estimated assuming a homogenous dye coverage using the experimental saturated dye density at the TiO_2 surface (Table 3). The effective area here considered is all the space at the TiO_2 surface unavailable for other dye molecules upon adsorption of one dye molecule. Porphyrins 1 and 2(opp) have the lowest A_{dye} values that, together with the splitting of the Soret band upon TiO_2 adsorption, are consistent with densely packed molecules adsorbed perpendicularly to the TiO_2 surface. The absence of splitting in the Ni complexes and their intermediate values of A_{dye} are in agreement with the tilted geometry presented in Figure 4. It is interesting to note that TPPCOOH, with a shorter anchor group, occupies more space at the surface than porphyrins 1 and 2(opp). The bulky porphyrin ring closer to the TiO_2 surface seems to prevent a high surface coverage. Porphyrin 3 (adj) occupies the largest Adye, although the Soret splitting is indicative of densely packed molecules on the TiO2 surface. Those two observations support an anchoring mode through the two adjacent carboxyl groups, occupying more space at the surface and leading to a lower surface density.

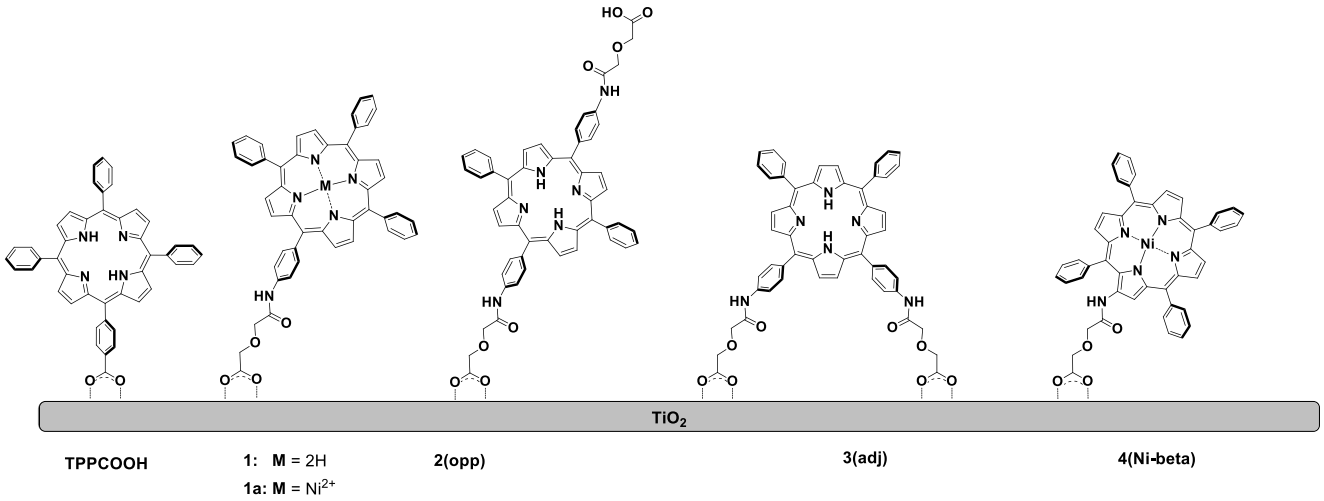

Fig. 4. Schematic view of the proposed adsorption geometry of porphyrin dyes on TiO_2 surface.

3.5. Photovoltaic performance

The performances of the devices with the various dyes are given in Table 4. The device efficiencies are somewhat low but it is widely recognized that solar cell efficiency depends strongly on the device fabrication conditions, and it is hard to directly compare the efficiencies reported by different research groups. The relevance of the efficiencies in Table 4 is mostly in revealing the relation between adsorption geometry and relative cell performance. Dye 1 yielded the best performing cell both using a liquid or a solid-state device. It outperforms the cell built with 3(adj) although there are reports in the literature of devices with dyes anchored by two linkers being more efficient and more stable than with one single linker.[41, 43, 79]

Table 4. Photovoltaic properties of porphyrin sensitized solar cells under 1.5 Sun, using: top rows) I^-/I^{3-} liquid-based electrolyte; bottom rows) spiro-OMeTAD polymeric hole conducting solid material.

Sensitizer	Fill factor / %	J_{SC} / mA cm^{-2}	V_{OC} / V	η / %	η_{rel} / %
1	60	3.08	0.44	0.81	0.81
1a(Ni)	63	1.26	0.47	0.37	0.62
2(opp)	34	0.17	0.27	0.02	0.02
3(adj)	63	2.04	0.41	0.53	1.12
4(Ni-beta)	63	1.22	0.46	0.35	0.61
1	53	0.36	0.61	0.12	0.12
3(adj)	41	0.35	0.62	0.09	0.19
4(Ni-beta)	43	0.05	0.54	0.01	0.02

For the liquid-base electrolyte cells, and with the exception of 1(opp), the fill factor and V_{OC} values are almost constant. Conversion efficiency follows the same trend as photocurrent generation, evaluated by J_{SC}, being this last factor determinant on the overall device conversion efficacy, η. A more insightful comparison of device efficiencies with different dyes should take into consideration the differences between surface coverage. Table 4 presents device efficiencies normalized for surface coverage leading to a molecular efficiency, η_{rel}, where the dye with the highest

surface coverage was taken as reference. As shown by the absorption spectra of porphyrins 1, 2(opp) and 3(adj) in Figure 1, Soret and Q bands have similar progression and relative intensities, thus the comparison between η_{rel} values is not contaminated by differences in spectral distribution of the photons. However, Table 1 shows that porphyrin 1 has the highest absorption coefficients of this series of dyes, which means that the η_{rel} values still have a bias towards device performance with dye 1. **Aditional to the fact that excited state deactivation is much faster,[65] also** the spectra and absorptivities of Ni porphyrins differ from those of the free-bases, and the comparison between them is not very informative.

Although high efficiency ruthenium dyes like N3 anchors on TiO_2 surface by two carboxyl groups, not many studies have been reported with porphyrins with two carboxyl anchors. Relevant work was done by C.-H. Hung and co-workers[41, 43] with porphyrins with carboxyphenyl groups at opposite (*trans*) and adjacent (*cis*) *meta* and *para* positions. Taking in account the loadings onto the TiO_2 surface, the double adjacent linkage to TiO_2 unequivocally yielded higher power conversion efficiencies.[43] It was concluded that charge recombination deleterious effects are higher in mono anchored dyes. The greater J_{SC} values observed and the dark current results seems to imply that a relative higher number of long-lived charges in the TiO_2 conduction band is achieved in cells sensitized with adjacently linked porphyrins.

Cell performance is dependent both on electron injection from the dye to the TiO_2 and the respective possibility of recombination. Both kinetics can be controlled by the dye-TiO_2 distance and should therefore respond to changes in dye-to-semiconductor distance. Reports considering through-bond electron transfer have used distinct spacer lengths in order to study the distance dependence, but limited correlation was observed.[80, 81] If we consider the possibility of through-space electron transfer, the *effective* distance in dye sensitized solar cells with porphyrins 1, 1(a)Ni, and 2(opp), should in fact correspond to a distance distribution related with the average distribution of molecular orientations on the TiO_2 surface. This distribution should somehow be restricted in dye 4(Ni-beta) and TPPCOOH, due to the shorter β linker, but the longer linker in the remaining dyes probably widens the possibility of "bending". On the other hand, the two linkers in the dye 3(adj) most likely restrict dye-TiO_2 conformation to a more rigid geometry.

Despite differences in redox potential and photophysics between metallated and non-metallated carboxylated porphyrin sensitizers it was been argued that the kinetics of electron injection and thus the efficiency of electron injection into the conduction band of TiO_2, are virtually similar for all those sensitizers (and even for the ruthenium polypyridyl N3 dye).[82, 83] The charge recombination dynamics was found to be controlled by the spatial separation from the dye cation to the TiO_2 surface.[77] Those observations imply that factors other than photophysics or electrochemistry may be of superior importance. These factors may be related to adsorption geometry, effective distance or aggregation effects. A relationship was found between cell efficiencies normalized for surface coverage, η_{rel}, and electron transfer dynamics at a molecular level.[39, 40] In cells sensitized by porphyrin dyes, η_{rel} is affected by multiple conditions related with adsorption geometry, namely by dye-TiO_2 surface distance. Efficiencies also depend critically on the molecular spacer connecting the porphyrin core to the TiO_2 surface, sensitization conditions (solvent and time) and the nature of the terminal group of the porphyrin.[39] The effect of adsorption geometry on cell efficiency was rationalized on the faster through-space electron recombination for dyes closer to the TiO_2 surface. In the present work we kept constant the adsorption solvent (THF as solvent with co-adsorbent chenodeoxyxcholic acid) and adsorption time (overnight adsorption), and focused on the specific adsorption geometry of the synthesized porphyrins on cell performance. The *molecular* efficiencies of both cells with Ni metals, 1a(Ni) and 4(Ni-beta) are similar, inducing that at this particular case the adsorption geometry by a β linker is not relevant, although this linker probably leads to a shorter distance.

An interesting result presented here is the fact that dyes 1 and 2(opp) have similar photophysical and electrochemical properties (with similar values of ΔG_{CS} and ΔG_{reg}) and yield similar dye coverage, but 2(opp) has a much worse device performance, yielding low values for both V_{OC} and J_{SC}. This drastic drop in efficiency was not observed for Zn-porphyrins linked to the TiO_2 surface by shorter phenyl spacer with monocarboxyl and dicarboxyl in opposite anchor groups.[43] It is possible that the long extra linkage has some anomalous "chemical" effect (i.e., binding to other nearby TiO_2 surfaces) that leads to much less *molecular* efficiency.

The comparison between dyes 1 and 3(adj), which have similar photophysical and electrochemical properties, is very informative. Dye 3(adj) has similar electron injection thermodynamics (ΔG_{CS}=-0.18 eV for dye 3(adj) and ΔG_{CS}=-0.20 for dye 1) but a higher η_{rel} than for dye 1. Dyes 1 and 2(opp) have tilt angles that bring then be closer to the TiO_2 surface and may enhance the electron recombination between TiO_2 conduction band and the dye cation, while 3(adj) keeps the porphyrin in a limited range of distances, far from the TiO_2 surface, limiting recombination. Through bond electron transfer would not explain the differences, as the spacer is the same on those dyes. Enhancing conduction band electrons lifetime would enhance cell *molecular* efficiency. This is consistent with a predominantly through-space electron transfer. For a linear through space transfer, higher static linear distance for dye 1 (please see Figure 4) would most probably slow the recombination rate and enhance the relative surface coverage normalized photocurrent generation (and η_{rel}) contrary to the observed. Consequently for through space electron transfers we have to take in account the possibility of tilting allowed by spacer flexibility and not only the distance considering a particular linear configuration. In the present case, where the anchor group is connected to the porphyrin core through a more extended glycolic acid spacer, the adsorption geometry effect seems to be even more relevant than for smaller spacers.[41, 43] The success of DSSCs based on Ru(II) complexes or porphyrins is partly due to their favorable kinetics of electron injection and recombination. Their electronic excited states inject electrons in the conduction band of nanocrystalline TiO_2 films in less than 25 ps, with almost indistinguishable electron injection kinetics,[82] giving charge separations efficiencies up to 98 %, while the recombination rates were found to be only weakly dependent on the nature of sensitizer.[82] Structural factors are known to have an impact in charge recombination.[22] For e.g. in a D–π–A organic sensitizer, by avoiding cations from approaching towards the TiO_2 surface an hexyl substituent on the π-bridge unit has a significant influence on the prevention of charge recombination.[7] The better performance of 3(adj), even under unfavorable thermodynamics for electron injection from the thermalized excited state, suggest that through-space electron recombination is hindered and overall determines device efficiency.

The photoelectrodes of ssDSSCs are 7-8 times thinner than those of DSSC with liquid electrolyte (1 μm vs 7-8 μm), to account for the reduced mobility of solid state HTMs. Hence, ssDSSCs have a lower amount of dye resulting in lower Jsc. and a higher V_{OC}. The data in Table 4 are consistent with previous reports. The molecular efficiencies (η_{rel}) of dyes 3(adj) and 1 in a solid-state device follow the same trend as in the presence of a liquid electrolyte. Again this may be assigned to ability of the second spacer-anchor group in 3(adj) to keep the dye backbone at a higher distance from TiO_2 than the single spacer-anchor group 1 during the process of coating the solid HTM onto the photoelectrode, and hinder electron recombination.

4. Conclusions

We compared the efficiencies of DSSCs with *meso*-tetraphenylporphyrins with a single *N*-glycolic acid amino anchoring group, with two anchoring groups in opposite (*trans)* and adjacent (*cis*) positions, and with the same anchoring group in a *beta* position. Photophysics, electrochemical and TiO_2 anchoring properties of the newly synthesized unsymmetrical *N*-glycolic acid amino phenyl porphyrins and their nickel metallocomplexes were evaluated.

Similarity in adsorption rates and surface coverage of 1 and 2(opp) suggests perpendicular adsorption to the TiO_2 surface, maximizing surface coverage. The lower surface density coverage of (3(adj)) reflects the use of two anchoring groups to adsorb to TiO_2 and flatter adsorption geometry. The measured cell efficiency normalized for surface coverage (η_{rel}) is higher for dye 3(adj) than for dye 1. We consider that porphyrin 1 tilting angles make the dye closer (on average) to the TiO_2 surface and enhance the electron recombination between TiO_2 conduction band and the dye cation, while 3(adj) keeps the porphyrin in a limited range of distances, far from the TiO_2 surface, limiting recombination. We conclude that the dye-TiO_2 effective distance in 3(adj) is more favorable for the electron injection/recombination rate relation needed to achieve high cell performance. The data obtained is consistent with a through-space electron transfer and confirm the relationship between cell efficiencies, adsorption geometry and effective distance between the dye core and TiO_2 surface, and electron transfer dynamics at a molecular level.

Acknowledgements

Work was performed under the project "SunStorage - Harvesting and storage of solar energy", reference POCI-01-0145-FEDER-016387, funded by European Regional Development Fund (ERDF), through COMPETE 2020 - Operational Programme for Competitiveness and Internationalisation (OPCI), and by national funds, through FCT (Fundação para a Ciência e a Tecnologia I.P, Portugal). The Coimbra Chemistry Centre (CQC) is supported by FCT through the program PEst-OE/QUI/UI0313/2014. ERDF through COMPETE and POCI-2010, and FCT support in part UC-NMR Lab by grants REEQ/481/QUI/2006, RECI/QEQ-QFI/0168/2012, CENTRO-07-CT62-FEDER-002012; and Coimbra Laser Lab by grant RNIE/0152/2013/022124. CJPM gratefully acknowledges FCT for a grant (SFRH/BD/37652/2007). MLD gratefully acknowledges Welsh Government funding for Sêr Solar Cymru and EPSRC/TSB funding for SPECIFIC (EP/N020863/1).

References

[1] B. O'Regan, M. Grätzel, *Nature* **1991**, *335*, 737.
[2] M. Grätzel, *J. Photochem. Photobiol. C: Photochem. Rev.* **2003**, *4*, 145.
[3] M. K. Nazeeruddin, E. Baranoff, M. Grätzel, *Solar Energy* **2011**, *85*, 1172.
[4] M. Grätzel, *Inorg. Chem.* **2005**, *44*, 6841.
[5] P. J. Holliman, M. Mohsen, A. Connell, M. L. Davies, K. Al-Salihi, M. B. Pitak, G. J. Tizzard, S.J. Coles, R. W. Harrington, W. Clegg, C. Serpa, O. H. Fontes, C. Charbonneau, M. J. Carnie, *J. Mater. Chem.* **2012**, *22*, 13318.
[6] S. Ito, S. M. Zakeeruddin, R. Humphry-Baker, P. Liska, R. Charvet, P. Comte, M. K. Nazeeruddin, P. Péchy, M. Takata, H. Miura, S. Uchida, M. Grätzel, *Adv. Mater.* **2006**, *18*, 1202.
[7] Y. K. Eom, S. H. Kang, I. T. Choi, Y. Yoo, J. Kim, H. K. Kim, *J. Mater. Chem.* **2017**, *5*, 2297.
[8] A. Connell, P. J. Holliman, M. L. Davies, C. D. Gwenin, S. Weiss, M. B. Pitak, P. N. Horton, S. J. Coles, G. Cooke, *J. Mater. Chem. A* **2014**, *2*, 4055.
[9] K. Hara, Z.-S. Wang, T. Sato, A. Furube, R. Katoh, H. Sugihara, Y. Dan-oh, C. Kasada, A. Shinpo, S. Suga, *J. Phys. Chem. B* **2005**, *109*, 15476.
[10] C. Li, J.-H. Yum, S.-J. Moon, A. Herrmann, F. Eickemeyer, N. G. Pschirer, P. Erk, J. Schoeneboom, K. Muellen, M. Grätzel, M. K. Nazeeruddin, *ChemSusChem* **2008**, *1*, 615.
[11] C. Li, Z. Liu, J. Schoneboom, F. Eickemeyer, N. G. Pschirer, P. Erk, A. Herrmann, K. Mullen, *J. Mater. Chem.* **2009**, *19*, 5405.
[12] S. Mori, M. Nagata, Y. Nakahata, K. Yasuta, R. Goto, M. Kimura, M. Taya, *J. Am. Chem. Soc.* **2010**, *132*, 4054.
[13] P. Y. Reddy, L. Giribabu, C. Lyness, H. J. Snaith, C. Vijaykumar, M. Chandrasekharam, M. Lakshmikantam, J. H. Yum, K. Kalyanasundaram, M. Grätzel, M. K. Nazeeruddin, *Angew. Chem. Int. Ed.* **2007**, *46*, 373.
[14] J.-J. Cid, J.-H. Yum, S.-R. Jang, M. K. Nazeeruddin, E. M. Ferrero, E. Palomares, J. Ko, M. Grätzel, T. Torres, *Angew. Chem. Int. Ed.* **2007**, *46*, 8358.
[15] J.-J. Guo, S.-R. Wang, X.-G. Li, F. Zhang, X.-N. Shao, X.-J. Lian, *J. Mol. Struct.* **2014**, *1060*, 17.
[16] F. Zhang, S.-R. Wang, X.-G. Li, Y. Xiao, J.-J. Guo, *J. Mol. Struct.* **2016**, *1107* 329.
[17] H. Shahroosvand, S. Zakavi, A. Sousaraeia, M. Eskandaria, *Phys. Chem. Chem. Phys.* **2015**, *17*.
[18] M. V. Martinez-Diaz, G. de la Torre, T. Torres, *Chemical Communications* **2010**, *46*, 7090.
[19] M. G. Walter, A. B. Rudine, C. C. Wamser, *J. Porphyr. Phthalocyanines* **2010**, *14*, 759.
[20] F. Odobel, E. Blart, M. Lagrée, M. Villieras, H. Boujtita, N. El Murr, S. Caramori, C. Alberto Bignozzi, *J. Mater. Chem.* **2003**, *13*, 502.

[21] J. Fernández-Ariza, M. Urbani, M. Gratzel, M. S. Rodríguez-Morgade, M. K. Nazeeruddin, T. Torres, *ChemPhotoChem* **2017**, *1*, 164.
[22] J.-M. Ji, H. Zhou, H. K. Kim, *J. Mater. Chem. A* **2018**, 14518.
[23] X. F. Wang, O. Kitao, H. Zhou, H. Tamiaki, S. Sasaki, *Chem. Commun.* **2009**, 1523.
[24] X. F. Wang, H. Tamiaki, L. Wang, N. Tamai, O. Kitao, H. Zhou, S. Sasaki, *Langmuir* **2010**, *26*, 6320.
[25] C. J. P. Monteiro, J. Pina, M. M. Pereira, L. G. Arnaut, *Photochem. Photobiol. Sci.* **2012**, *11*, 1233.
[26] H. Scheer, in *Chlorophylls and Bacteriochlorophylls: Biochemistry, Biophysics, Functions and Applications* (Eds.: B. Grimm, R. J. Porra, W. Rüdiger, H. Scheer), Spinger, **2006**, pp. 1.
[27] X.-F. Wang, O. Kitao, H. Zhou, H. Tamiaki, S.-I. Sasaki, *J. Phys.Chem. C* **2009**, *113*, 7954.
[28] S. Mathew, A. Yella, P. Gao, H.-B. R., C. B. F. E., A.-A. N., T. I., U. Rothlisberger, N. M. K., M. Gratzel, *Nat. Chem.* **2014**, *6*, 242.
[29] A. Yella, H.-W. Lee, H. N. Tsao, C. Yi, A. K. Chandiran, M. K. Nazeeruddin, E. W.-G. Diau, C.-Y. Yeh, S. M. Zakeeruddin, M. Grätzel, *Science* **2011**, *334*, 629.
[30] S. H. Kang, M. J. Jeong, Y. K. Eom, I. T. Choi, S. M. Kwon, Y. Yoo, J. Kim, J. Kwon, J. H. Park, H. K. Kim, *Adv. Energy Mater.* **2017**, 1602117.
[31] M. Urbani, M. Grätzel, M. K. Nazeeruddin, T. Torres, *Chem. Rev.* **2014**, *114*, 12330.
[32] T. Higashino, H. Imahori, *Dalton Trans.* **2015**, *44*, 448.
[33] C. J. P. Monteiro, M. M. Pereira, M. G. H. Vicente, L. G. Arnaut, *Tetrahedron* **2012**, *68*, 8783.
[34] W. M. Campbell, A. K. Burrell, D. L. Officer, K. W. Jolley, *Coord. Chem. Rev.* **2004**, *248*, 1363.
[35] H. Imahori, T. Umeyama, S. Ito, *Acc. Chem. Res.* **2009**, *42*, 1809.
[36] Q. Wang, W. M. Campbell, E. E. Bonfantani, K. W. Jolley, D. L. Officer, P. J. Walsh, K. Gordon, R. Humphry-Baker, M. K. Nazeeruddin, M. Grätzel, *J. Phys. Chem. B* **2005**, *109*, 15397.
[37] M. Ishida, S. W. Park, D. Hwang, Y. B. Koo, J. L. Sessler, D. Y. Kim, D. Kim, *Journal of Physical Chemistry C* **2011**, *115*, 19343.
[38] W. M. Campbell, K. W. Jolley, P. Wagner, K. Wagner, P. J. Walsh, K. C. Gordon, L. Schmidt-Mende, M. K. Nazeeruddin, Q. Wang, M. Grätzel, D. L. Officer, *J. Phys. Chem. C* **2007**, *111*, 11760.
[39] S. Ye, A. Kathiravan, H. Hayashi, Y. Tong, Y. Infahsaeng, P. Chabera, T. r. Pascher, A. P. Yartsev, S. Isoda, H. Imahori, V. Sundströ̈m, *J. Phys. Chem. C* **2013**, *117*, 6066−6080.
[40] H. Imahori, S. Kang, H. Hayashi, M. Haruta, Hiroki Kurata, S. Isoda, S. E. Canton, Y. Infahsaeng, A. Kathiravan, T. Pascher, P. Chábera, A. P. Yartsev, V. Sundströ̈m, *J. Phys. Chem. A* **2011**, *115*, 3679.
[41] R. B. Ambre, S. B. Mane, G.-F. Chang, C.-H. Hung, *ACS Appl. Mater. Interfaces* **2015**, *7*, 1879−1891.
[42] M. K. Panda, G. D. Sharma, K. R. J. Thomasd, A. G. Coutsolelos, *J. Mater. Chem.* **2012**, *22*, 8092.
[43] R. Ambre, K.-B. Chen, C.-F. Yao, L. Luo, E. W.-G. Diau, C.-H. Hung, *J. Phys. Chem. C* **2012**, *116*, 11907−11916.
[44] L. G. Arnaut, M. Barroso, C. Serpa, in *Applied Photochemistry*, 1 ed. (Eds.: P. Douglas, H. D. Burrows, R. Evans), Springer-Verlag, Dordrecht, **2013**, pp. 267.
[45] M. M. Pereira, C. J. P. Monteiro, A. V. Simões, S. M. A. Pinto, A. R. Abreu, G. F. F. Sa, E. F. F. Silva, L. B. Rocha, J. M. Dabrowski, S. J. Formosinho, S. Simões, L. G. Arnaut, *Tetrahedron Lett.* **2010**, *66*, 9545.
[46] D. D. Perrin, W. L. F. Armarego, D. R. Perrin, *Purification of Laboratory Chemicals*, 2nd ed., Pergamon Press, Oxford, **1980**.
[47] R. A. W. Johnstone, M. Nunes, M. M. Pereira, A. Gonsalves, A. C. Serra, *Heterocycles* **1996**, *43*, 1423.
[48] A. M. A. R. Gonsalves, J. M. T. B. Varejão, M. M. Pereira, *J. Heterocyclic Chem.* **1991**, *28*, 635.
[49] M. Sibrian-Vazquez, T. J. Jensen, M. G. H. Vicente, *J. Photochem. Photobiol., B: Biol.* **2007**, *86*, 9.
[50] A. D. Adler, F. R. Longo, F. Kampas, J. Kim, *J Inorg Nucl Chem* **1970**, *32*, 2443.
[51] M. Sibrian-Vazquez, T. J. Jensen, R. P. Hammer, M. G. H. Vicente, *Journal of Medicinal Chemistry* **2006**, *49*, 1364.
[52] M. Sibrian-Vazquez, T. J. Jensen, M. G. H. Vicente, *J. Photochem. Photobiol., B* **2007**, *86*, 9.
[53] A. F. Peixoto, D. S. de Melo, T. F. Fernandes, Y. Fonseca, E. V. Gusevskaya, A. M. S. Silva, R. R. Contreras, M. Reyes, A. Usubillaga, E. N. dos Santos, M. M. Pereira, J. C. Bayon, *Appl. Catal., A* **2008**, *340*, 212.
[54] S. L. Murov, I. Carmichael, G. L. Hug, *Handbook of Photochemistry* 2nd ed., CRC Press, New York, **1993**.
[55] J. Pina, J. S. de Melo, H. D. Burrows, A. L. Maçanita, F. Galbrecht, T. Buennagel, U. Scherf, *Macromolecules* **2009**, *42*, 1710.
[56] E. E. Beauvilliers, T. Malewschik, G. J. Meyer, *ChemPhotoChem* **2017**, *1*, 415.
[57] A. Kathiravan, R. Renganathan, *J Colloid Interface Sci* **2009**, *331*, 401.
[58] E. Galoppini, *Coord. Chem. Rev.* **2004**, *248*, 1283.
[59] K. Kalyanasundaram, M. Grätzel, *Coord. Chem. Rev.* **1998**, *177*, 347.
[60] A. Forneli, M. Planells, M. A. Sarmentero, E. Martinez-Ferrero, B. C. O'Regan, P. Ballester, E. Palomares, *J. Mater. Chem.* **2008**, *18*, 1652.
[61] A. Giraudeau, H. J. Callot, J. Jordan, I. Ezhar, M. Gross, *J. Am. Chem. Soc.* **1979**, *101*, 3857.
[62] L. Jaquinod, in *The Porphyrin Handbook, Vol. 1* (Eds.: K. M. Kadish, K. M. Smith, R. Guilard), Academic Press, San Diego, **2000**, pp. 201.
[63] W. J. Kruper, T. A. Chamberlin, M. Kochanny, *J. Org. Chem.* **1989**, *54*, 2753.
[64] R. K. Sharma, G. Ahuja, I. T. Sidhwani, *Green Chem. Lett. Rev.* **2009**, *2*, 101.
[65] L. G. Arnaut, in *Adv. Inorg. Chem., Vol. 63* (Ed.: R. S. G. VanEldik), Elsevier, **2011**, pp. 187.
[66] M. Gouterman, in *The Porphyrins, Vol. III* (Ed.: D. Dolphin), Academic Press, **1978**.
[67] M. Ishida, D. Hwang, Z. Zhang, Y. J. Choi, J. Oh, V. M. Lynch, D. Y. Kim, J. L. Sessler, D. Kim, *ChemSusChem* **2015**, *8*, 2967.
[68] T. L. C. Figueiredo, R. A. W. Johnstone, A. Sorensen, D. Burget, P. Jacques, *Photochem. Photobiol. Sci.* **1999**, *69*, 517.
[69] J.-J. Guo, E. S.-R. Wang, X.-G. Li, F. Zhang, Y. Xiao, C. Teng, *Aust. J. Chem.* **2015**, *68*, 1025.
[70] T. D. Santos, A. Morandeira, S. Koops, A. J. Mozer, G. Tsekouras, Y. Dong, P. Wagner, G. Wallace, J. C. Earles, K. C. Gordon, D. Officer, J. R. Durrant, *J. Phys. Chem. C* **2010**, *114*, 3276.
[71] P. V. Kamat, M. Haria, S. Hotchandani, *J. Phys. Chem. B* **2004**, *108*, 5166.

[72] S. Eu, S. Hayashi, T. Urneyama, Y. Matano, Y. Araki, H. Imahori, *Journal of Physical Chemistry C* **2008**, *112*, 4396.
[73] M. Juozapavicius, M. Kaucikas, J. J. v. Thor, B. C. O'Regan, *J. Phys. Chem. C* **2013**, *117*, 116.
[74] J. Kallioinen, G. Benko, V. Sundstrom, J. E. I. Korppi-tommolas, A. P. Yartsev, *J. Phys. Chem. B* **2002**, *106*, 4396.
[75] H. Imahori, S. Hayashi, H. Hayashi, A. Oguro, S. Eu, T. Umeyama, Y. Matano, *J. Phys. Chem. C* **2009**, *113*, 18406.
[76] C.-F. Lo, S.-J. Hsu, C.-L. Wang, Y.-H. Cheng, H.-P. Lu, E. W.-G. Diau, C.-Y. Lin, *J. Phys. Chem. C* **2010**, *114*, 12018.
[77] S. Eu, S. Hayashi, T. Umeyama, A. Oguro, M. Kawasaki, N. Kadota, Y. Matano, H. Imahori, *J. Phys. Chem. C* **2007**, *111*, 3528.
[78] H. Imahori, Y. Matsubara, H. Iijima, T. Umeyama, Y. Matano, S. Ito, M. Niemi, N. V. Tkachenko, H. Lemmetyinen, *J. Phys. Chem. C* **2010**, *114*, 10656.
[79] A. Connell, P. J. Holliman, E. W. Jones, L. Furnell, C. Kershaw, M. L. Davies, C. D. Gwenin, M. B. Pitak, S. J. Coles, G. Cooke, *J. Mater. Chem. A* **2015**, *3*, 2883.
[80] S. Ardo, G. J. Mayer, *Chem. Soc. Rev.* **2009**, *38*, 115.
[81] K. Kilså, E. I. Mayo, D. Kuciauskas, R. Villahermosa, N. S. Lewis, J. R. Winkler, H. B. Gray, *J. Phys. Chem. A* **2003**, *107*, 3379.
[82] Y. Tachibana, S. A. Haque, I. P. Mercer, J. R. Durrant, D. R. Klug, *J. Phys. Chem. B* **2000**, *104*, 1198.
[83] J. N. Clifford, E. Palomares, M. K. Nazeeruddin, M. Grätzel, J. Nelson, X. Li, N. J. Long, J. R. Durrant, *J. Am. Chem. Soc.* **2004**, *126*, 5225.